SCANNING Vol. 16, 78–86 (1994)

Received October 19, 1993

Quantitation of SEM EBIC and CL Signals Using Monte Carlo Electron-Trajectory Simulations

D.B. HOLT AND E. NAPCHAN

Imperial College of Science, Technology and Medicine, Department of Materials, London, UK

Summary: A microcomputer Monte Carlo program simulates electron trajectories in solids and describes the distribution of energy deposited throughout the energy-dissipation (electron-hole pair generation) volume. From this distribution, the electron-beam-induced current or cathodoluminescence signal that will be generated can be calculated for the chosen beam conditions in a multilayer specimen of any geometry and compositions. The use of this program is illustrated by applications (1) to simulate curves of cathodoluminescence intensity versus beam energy for fitting to experimental data to evaluate materials and device parameters, (2) to calculate the energy deposited in each layer of a HEMT structure in which electron-beam-induced current studies are in progress, and (3) to the simulation of defect contrast linescan profiles which are compared to experimental observations.

Key words: cathodoluminescence, Monte Carlo electron-trajectory simulations, electron-beam-induced current

Introduction

The only effective method for quantifying the modes of the scanning electron microscope (SEM) is the use of Monte Carlo electron-trajectory simulations. Monte Carlo methods were introduced by von Neumann for problems arising in the wartime atomic bomb project. In the 1950s and early 1960s Monte Carlo electron-trajectory simulations were introduced to help quantify electron probe x-ray microanalysis (Bishop 1964). Later Yakowitz and coworkers at the American National Bureau of Standards (NBS) developed a simplified "plural scattering" model that enabled electron-trajectory simulations to be run on the microcomputers that were just becoming available (Myklebust *et al.* 1976, Newbury 1989). Joy and coworkers applied this approach to quantify EBIC (electron-beam-induced current) and dislocation contrast using the Donolato phenomenological model (Czyzewski and Joy 1991, Joy and Pimentel 1983).

A Monte Carlo simulation shows the depth of penetration and, hence, the depth resolution and shows the lateral spreading and the lateral spatial resolution of the beam in the bulk modes. It also provides data on the three-dimensional distribution of beam energy within the specimen.

A program derived from the NBS—Joy programs was written to deal with epitaxial multilayer materials like those typical of III-V optoelectronic devices (Napchan 1988, Napchan and Holt 1987). The unique value of the Monte Carlo simulation method lies in its ability to deal with experimental situations for which no explicit mathematic representations are available. Common examples include the epitaxial multilayer materials mentioned above, cases in which the beam is not incident normally, and device structures that are laterally limited so the beam scans across heterojunctions, for example, or the edges of quantum wires, etc. This package of programs has now been considerably enhanced, and this paper reports the latest developments and illustrates them with examples of recent experimental applications.

Address for reprints:

D.B. Holt
Imperial College of Science, Technology and Medicine
Department of Materials
Prince Consort Road
London SW7 2BP, UK

MC-SET

The latest versions of the program are now called MC-SET (Monte Carlo simulation of electron trajectories). MC-SET is now written in the C programming language, and a menu driven user interface makes it

easy to use. It allows the specification of specimens that contain laterally limited device structures as well as many layers of different materials. It includes EBIC and CL (cathodoluminescence) signal strength and defect contrast calculations, using simplified models. It will repeat calculations for any of the specified EBIC or CL materials and device parameters over a chosen range for a selected value step.

The MC-SET simulation results are stored in a two-dimensional matrix, a coordinate of which is the depth. This describes the laterally or radially integrated energy deposition in the specimen. The size of this matrix is 80 by 80 elements and the relationship to the sample dimensions of interest is set up according to the experimental conditions, usually to cover the penetration depth of the beam electrons. Figure 1 shows a typical result of an MC-SET simulation. The screen automatically displays (Fig. 1a) not only a plot of the first 200 trajectories calculated, but also depth- and lateral-dose plots for the total number calculated, which was 3000 in this case. (Plotting more than a few hundred trajectories would obscure all detail, but thousands of trajectories must be calculated to give statistically reliable energy dissipation data, such as depth dose plots.) The depth dose is the energy deposited per unit of depth; it is plotted versus depth in the central panel. The lateral dose is the energy dissipated in lamellae parallel to the zy plane (where z is the depth dimension), and it is plotted versus x from the beam-impact point at the position of the sharp peak. The program also provides a graphic display of the energy deposited in each of the materials of a multilayer sample (Fig. 1c). This is given as a percentage of the total beam energy, nE_b where n is the number of electrons for which trajectories have been calculated and Eb is the energy of an incident beam electron in keV. The numbers of secondary and backscattered electrons as a percentage of the beam electrons and the energies of these emissions are also printed out at the top of these graphics screens.

CL Modeling

Monte Carlo calculations of CL contrast and of CL signal strength were first carried out by Czyzewski and Joy (1990) and by Phang *et al.* (1992), respectively. The latter used a sophisticated model and a mainframe computer.

The CL modeling using the MC-SET energy-deposition data is based on the following approach. From the energy deposition matrix the energy is further integrated along a second coordinate. The result is the description of the calculated three-dimensional energy deposition as an array of 80 elements [values of E(z), the energy deposited by the beam as a function of depth] along the beam penetration direction, z. This is, in fact, the depth-dose function for normal beam-incidence conditions and for symmetric specimen cross-sections.

To find the emitted CL intensity a series of calculations must be carried out as follows. For each point the number of resultant hole-electron pairs is arrived at by

$$n_{h-e} = E(z)/e_i, \tag{1}$$

where e_i is the h-e pair formation energy. The number of h-e pairs times the radiative recombination probability, η_r, times a half is the number of photons, n_{ph}, emitted up toward the exit surface. These are absorbed according to Lambert's law:

$$L(z) = L_0 \exp(-\alpha z), \tag{2}$$

where L_0 is the initial light intensity, α is the absorption coefficient, and L(z) is the light intensity remaining after propagating a distance z. (The value of α found by curve fitting for panchromatic CL data will be an effective value. In many cases the emitted CL consists essentially of the relatively narrow fundamental or near-band-edge emission. In such cases α will be the fundamental absorption-band value found just above the absorption edge.) The CL undergoes total internal reflection at the free (exit) surface so only a small fraction passes through. The light that is not totally internally reflected (and assumed lost) undergoes (partial) Fresnel reflection.

This is perhaps the point at which to emphasise the difference between the traditional theoretic approach and that of computer simulation. To give a theoretic treatment, one tries to take account of all the physical phenomena involved as realistically as possible. Any physical parameter values used will be carefully selected from the best data available. A body of literature applies this approach with considerable success to SEM CL problems [see Yacobi and Holt (1990) for references]. In the case of microcomputer simulation for the laboratory, however, one must use the simplest possible model to get an algorithm that will run reasonably quickly on a machine of limited speed and memory.

Comparison of the general form of the simulated curves with experimental data soon shows whether the phenomena that have been neglected can be ignored for practical purposes. If they can (when the simulated curves are of the experimentally observed form), it may be that they are negligible in fact or that the factors that have been omitted happen to cancel. Sets of simulated curves can then be rapidly calculated for ranges of values of the physical parameters involved, and comparison with experimental data gives best-fit values for these. This means that one can tackle materials and devices for which important parameter values are unknown, unreliable, or known to vary

widely. At the end of such work, one attempts to determine whether the best-fit values make sense regarding data from the literature, theoretic considerations, and extrapolation from related materials, or whether one looks for hypotheses that would account for the values that have been found.

Initial results for bulk material are as expected. Figure 2 shows the graphic result of the MC-SET simulation of a 20 keV beam incident normally on GaAs. A set of such electron trajectory simulations were run to produce depth-dose data as a function of beam voltage for a constant beam current (a constant number of electron trajectories simulated). These were used to calculate the values of the CL intensity emitted from bulk GaAs for a range of values of the absorption coefficient, α, shown in Figure 3a. For a constant beam current, the beam power increases linearly with E_b, the energy of the beam electrons in keV (the "beam energy"). This results in a linear increase in the number of photons generated in uniform material. In addition, however, the penetration depth increases with beam energy, roughly as E_b^n where $n \approx 1.75$. Hence, absorption results in losses that increase with E_b. Figure 3a demonstrates that large values of the absorption coefficient, α, lead to a decrease in CL emission intensity with E_b beyond a peak value. For small α values, however, the effect is only to produce a sub-linear increase over the range of beam energies available in SEMs. When there is a maximum in the curve of CL intensity as a function of beam energy, $L_{CL}(E_b)$, use of E_b values greater than that for the maximum is particularly undesirable. The CL signal strength is diminished, and the lateral spatial resolution is made worse. Use of higher E_b values would be justified only to penetrate to a deeper layer of material or defect.

Figure 3b shows the effect of varying dead layer thicknesses in the calculations for $\alpha = 0.8\ \mu m^{-1}$. For beam energies giving penetrations less than the dead-layer thickness, no emission is produced and the normal increase begins for greater beam energies. Experimentally, this effect is seen in its simplest form in ZnS where most of the radiation is extrinsic, with wavelengths to which the material is transparent, so $\alpha \approx 0$. The results from one particular crystal are shown in Figure 4. This behaviour has been known since the earliest studies of phosphor CL and is expressed by the relation:

$$L_{CL} = kf(I_b)(V_b - V_d)^m, \qquad (3)$$

where k is a constant, f represents the variation of intensity with beam current, L_{CL} is the CL intensity, V_d is the dead voltage (required to penetrate through the dead layer of thickness t_d), I_b and V_b the beam current

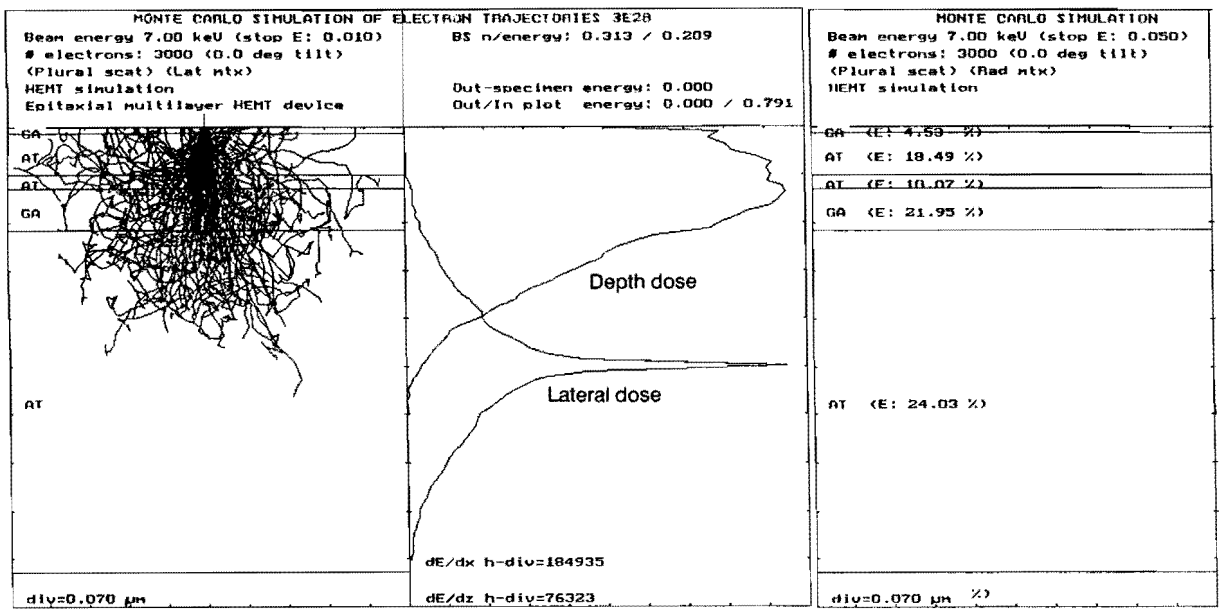

(a) (b) (c)

FIG. 1 (a) Trajectory plot, (b) depth- and lateral-dose plots, and (c) percentage of the total beam energy deposited in each layer of an epitaxial multilayer HEMT structure for a 7 keV electron beam. GA marks layers of GaAs and AT marks layers of $Al_{0.3}Ga_{0.7}As$. Depth on the vertical scales is in units of 0.070 μm. In the centre are plotted the depth dose E(z) in units of 184,935 eV per division. The lateral dose E(x) is in units of 76,323 eV per division, and the vertical scale represents the horizontal distance x in units of 0.070 μm. The right hand panel plots, for each layer of this HEMT structure, the percentage of the total beam energy (2.1×10^8 eV for the 3000 electrons each of 7 keV, for which trajectories were calculated) deposited in that layer.

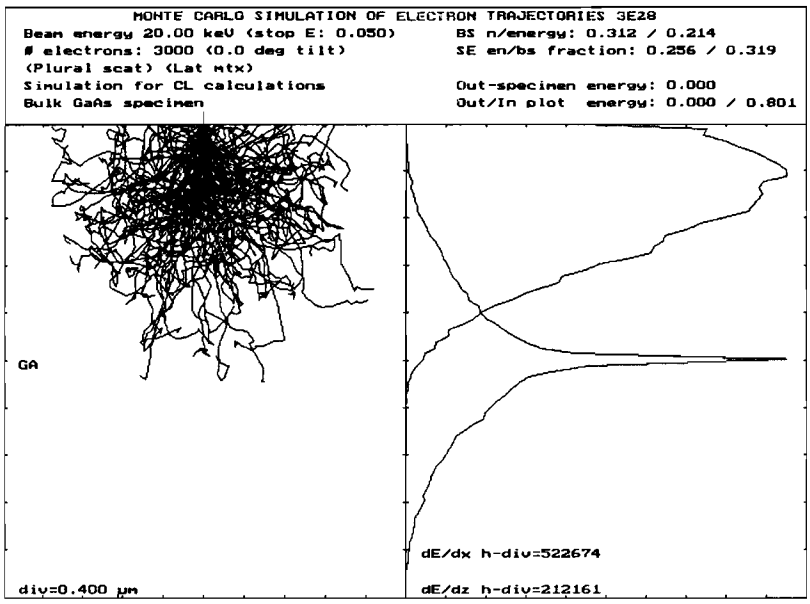

FIG. 2 MC-SET simulation display for a 20 keV beam and a bulk GaAs specimen. The values of the vertical and horizontal scale divisions are shown in the same way as on Figure 1.

and voltage, and m generally lies between 1 and 2 but can be up to 3 (Garlick 1949). With m = 1, this relation was known as Lennard's Law in the early phosphor CL literature. The results in Figure 4 fit linear and square laws (m = 1 and 2) about equally. This shows why the two expressions were in common use. Of course, in principle, one could test between them by measurements at lower beam voltages, but the CL intensity becomes too low to detect easily, particularly as the dead-layer effect becomes more important at low voltages. The linear plot gives $V_d = 15$ kV, corresponding to $t_d \approx 1.1$ μm (taking t_d = the Gruen range in ZnS for 15 kV). The dead layer is now assumed to be due to surface charges producing a field in a subsurface depletion region. This field separates the h-e pairs preventing them from recombining to produce light.

Surface recombination has been neglected in this discussion because often it is found to be overridden by the dead-layer effect. This arises because of surface-state trapping leading to a surface charge and subsurface depletion layer, as discussed above. This effect was first found in the early work on ZnS phosphors and is known to be important in some III-V materials as well.

Figures 5a,b are plots of experimental data on the integral CL-emitted intensity as a function of beam energy for two samples of bulk LEC InP material doped with Cr and Fe, respectively. The intensities were obtained as the output of Si photodetectors looking directly down on the specimen, that is, the ECL (emission CL) signal, measured as short circuit current in the one case and as open circuit voltage in

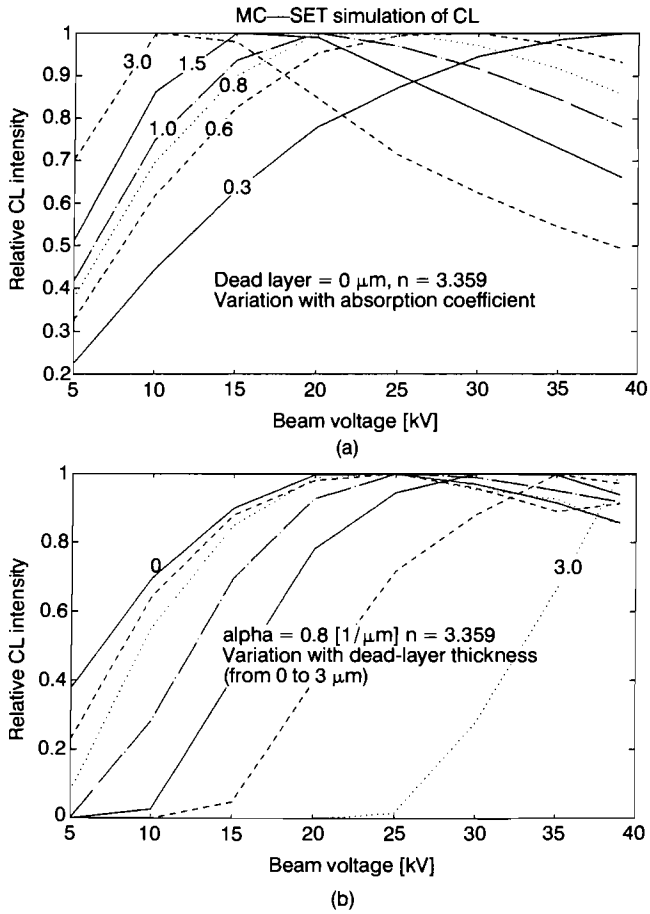

FIG. 3 Calculated CL intensities normalised to unity for the maximum intensity emitted from bulk GaAs for (a) values of absorption coefficient, α, from 0.3 to 3.0 μm^{-1} and zero dead-layer thickness, and (b) for dead-layer thicknesses from 0 to 3 μm and $\alpha = 0.8\ \mu m^{-1}$.

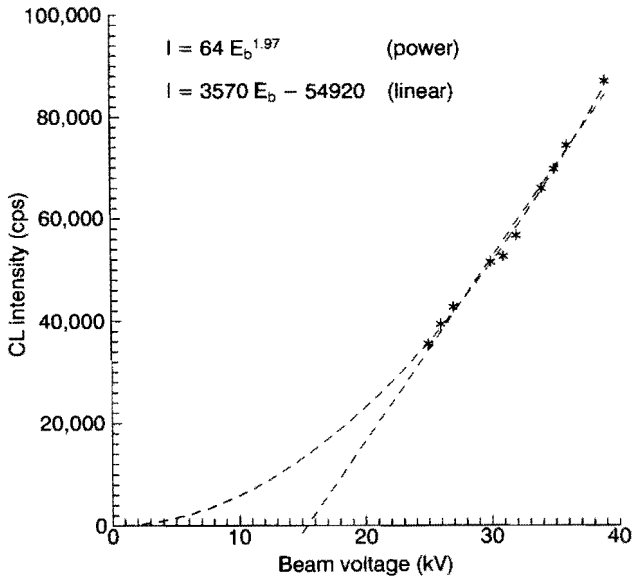

FIG. 4 Experimental values of the integral extrinsic CL intensity from a ZnS crystal, measured as total count rate with the monochromator of a spectral detection system set to the zero order, versus beam voltage. The curve and straight line show that the results, over the readily measurable range, fit first- and, approximately, second-power expressions comparably well.

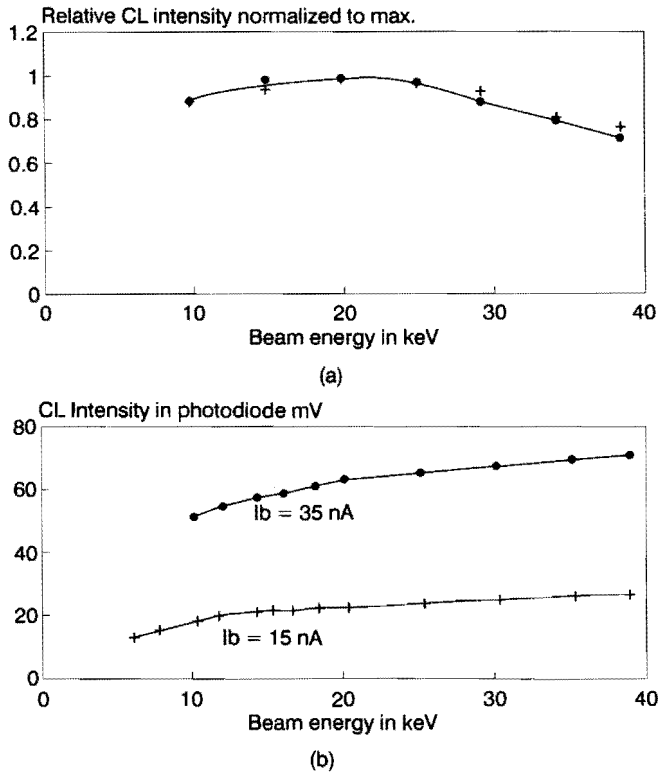

FIG. 5 Variation of the emitted CL intensity for LEC InP samples with beam energy in keV for constant beam currents for (a) Cr-doped and (b) Fe-doped material. The two sets of data (dots and plus signs) are for different values of beam current in each case.

the other. The response intensity is linear in each case. Notable is that by comparison with Figure 3a the data correspond to materials with a relatively large and a small absorption coefficient, respectively. This observation fits in with previous observations of dot-and-halo contrast at dislocations in the these materials (Holt *et al.* 1990). This is because of the precipitation of impurities on dislocations, producing dark dots in CL micrographs, and a bright denuded zone, or halo, around the dislocation. The effect was very strong in InP:Cr suggesting that Cr doping gives strong CL absorption. This form of contrast was much weaker in InP:Fe, suggesting that the increase in the absorption coefficient due to Fe doping was much less.

Dislocation CL Contrast

Only a few papers are available on the analysis of CL dark-dislocation contrast. Lohnert and Kubalek (1983, 1984) applied the Donolato phenomenological model to dark CL contrast. This model, originally for EBIC contrast, represents any defect as a volume of appropriate geometry in which the minority carrier lifetime is reduced. A dislocation is thus a circular cylinder of radius r_D. To account for CL dark contrast, the nonradiative recombination time and therefore the minority carrier lifetime are decreased inside the cylinder. This reduces the CL efficiency locally. This model apparently produced the required results.

Pasemann and Hergert (1986) and Jakubowicz (1986) independently realised that on the basis of the Donolato model the CL and EBIC dislocation dark-line contrasts are similar, with one exception: the depth dependence of the CL contrast, due to self-absorption, which has no EBIC analogue. It follows

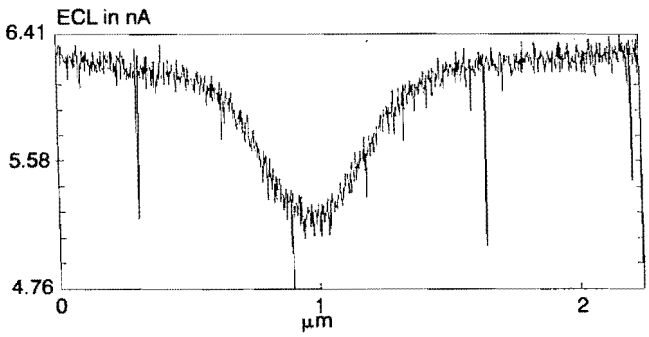

FIG. 6 Experimental CL line scan profile for a beam-induced dislocation. This ECL (emission CL) signal was detected by a Si photodiode set to view the specimen from above and was recorded as a current. CL of all wavelengths can be detected by this means, but spectroscopic observations showed the emission from this specimen to consist only of the near-band-edge emission ($h\nu \approx E_g$, the band gap energy).

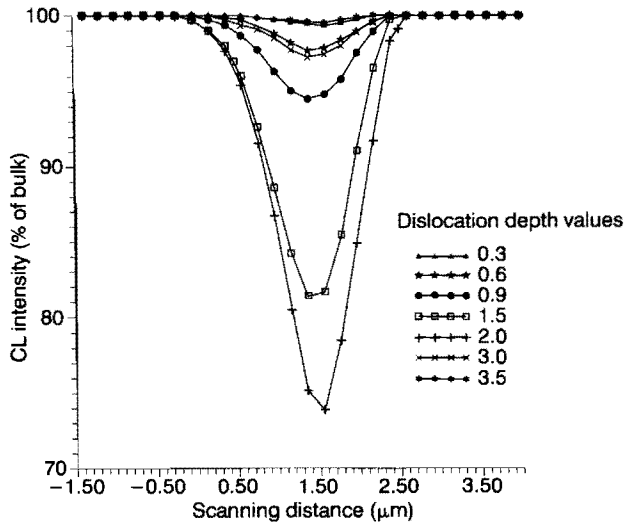

FIG. 7 A family of simulated contrast profiles for a dislocation of radius 0.5 μm in which 50% of the minority carriers are lost by recombination and running parallel to the surface at depths from 0.3 to 3.5 μm. These profiles were calculated for GaAs and a beam energy of 20 keV. The greatest reduction in CL intensity, that is, the greatest CL contrast is found for a depth of approximately 2 μm for this beam energy.

that the ratio of the two forms of contrast can be used to determine the dislocation depth (Jakubowicz *et al.* 1987).

Our aim is to make defect CL contrast analysis available to experimentalists in a form that is convenient for the determination of dislocation recombination strengths. The hope is that this will facilitate studies of the variations of defect CL properties, with material, type of dislocation, decoration, temperature, etc.

Dislocations can be induced in GaAs and InP by the high-beam currents that are sometimes needed for CL studies (Salviati *et al.* 1990). These dislocations are very suitable experimental objects as they are long and straight and run parallel to and just below the specimen surface. Moreover they are interesting in themselves as they run in <110> directions with [001] Burgers vector normal to the surface of the wafers and are apparently produced by a new mechanism (Holt *et al.* 1993). By selecting from among such dislocations, those that are widely separated from their neighbours, high-resolution CL line-scan profiles can readily be recorded for comparison with MC-SET simulated curves (Fig. 6).

In the present calculations of dark CL defect contrast, the dislocations are represented by cylinders of radius r_D inside which a percentage, p, of the minority carriers are lost by additional nonradiative recombination. The cylinder lies at a depth z_D and contrast linescan profiles can be simulated for ranges of values of r_D, p and z_D. Fitting experimental data to a family of calculated curves like that shown in Figure 7 gives values for these parameters for the particular dislocation. This simplified model is that previously used for EBIC (Norman and Holt 1989) except that, because of absorption, the contrast of dislocations in CL falls steadily with increasing z_D.

Multilayer and Device Structure Modeling

As an illustration of a phenomenon requiring the application of MC-SET to a multilayer device struc-

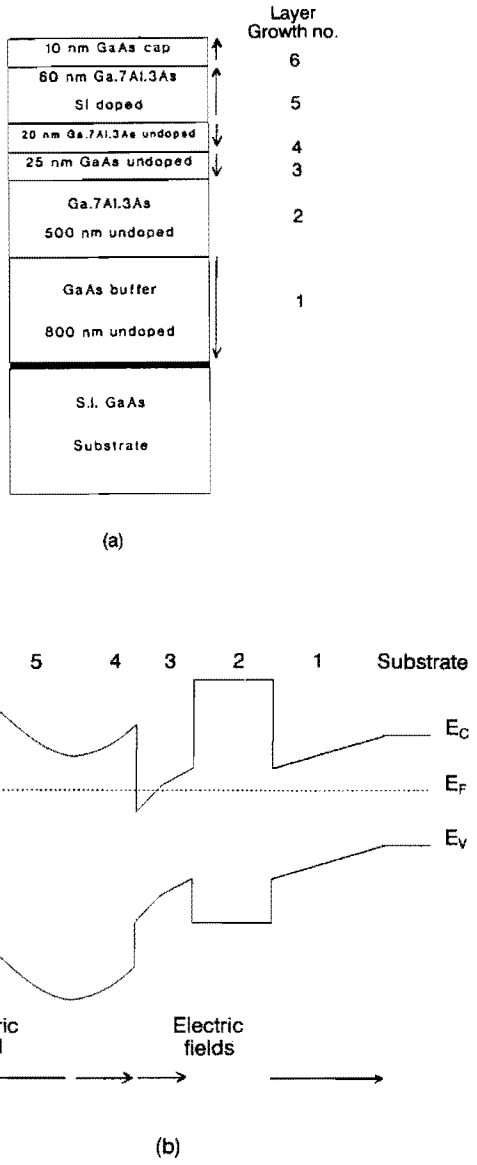

FIG. 8 The epitaxial layer structure of a HEMT wafer grown at LPSES (Laboratoire de Physique du Solide et Energie Solaire–CNRS, Valbonne, France) and (b) the energy-band diagram for this structure (Holt *et al.* 1993). The arrows are the directions of the built-in fields in the layers.

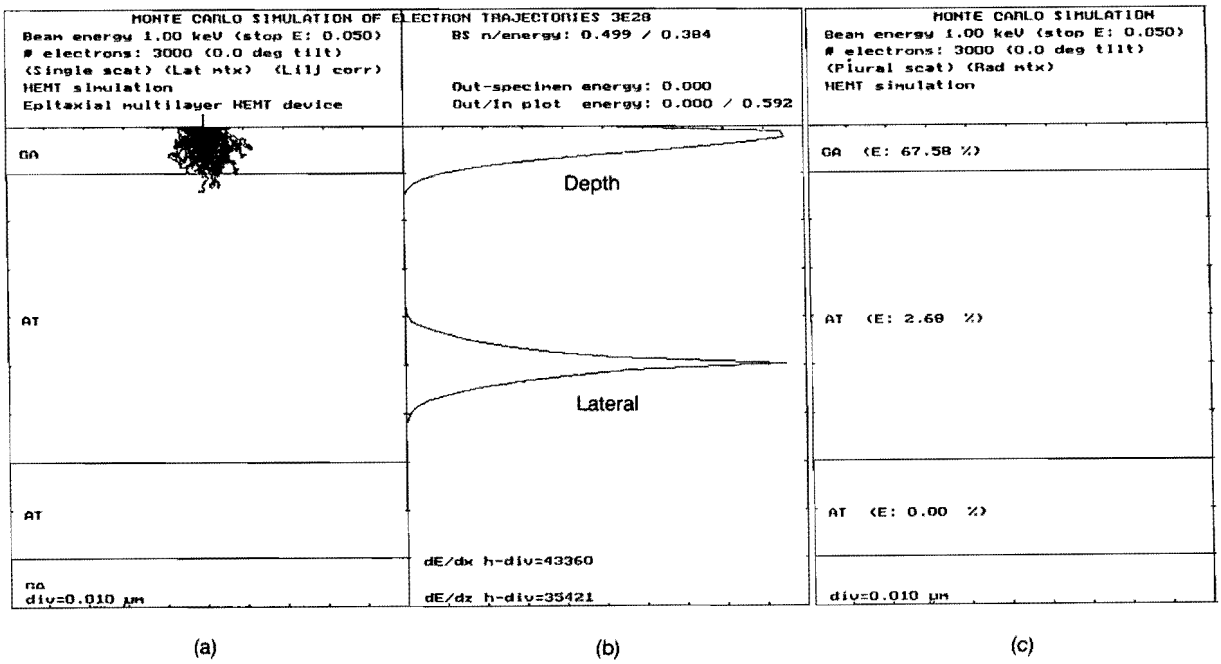

FIG. 9 Electron trajectories and energies deposited in the HEMT structure layers for a beam voltage of 1 kV. The values of the vertical and horizontal scale divisions are shown as for Figure 1. Comparison of Figures 9 and 1 shows how the deeper layers are increasingly excited as the beam energy increases.

ture, some results of EBIC observations on a HEMT structure are presented (Holt *et al.* 1993). The structure of these specimens is shown in Figure 8 and MC-SET graphics results for this structure in Figures 1 and 9. EBIC observations were carried out on specimens cut from a wafer with the structure of Figure 8 simply by applying silver paint contacts to the bottom and a point on the top. Charge collection relied on internal electric fields in the structure. The top layers, 5 and 6, have built-in fields collecting current upwards, that is, sending holes to the top contact and three deeper layers; numbers 4, 3 and 1 have fields collecting current downwards (Fig. 8). When care is taken to avoid beam damage, the variation of EBIC current between contacts to the top and bottom of the wafer varies with the beam voltage as shown in Figure 10 (Holt *et al.* 1993). The EBIC current reverses direction for beam voltages greater than about 5 kV as the beam penetrates through the shallow, upward-current layers and begins to generate h-e pairs in the deeper, downward-current charge-collecting layers. The simulations of Figures 1 and 9 are those for 1 and 7 keV beams. Experimentally, the EBIC currents for these beam energies are about equal and opposite in direction. The results of the simulations show that for 1 keV the h-e pair generation is entirely in the shallow, upward-current-collecting layers, while for 7 keV it is predominantly in the deeper, downward-current-collecting layers, which accounts for the reversal of direction of the observed EBIC current.

A second example of a device to which MC-SET is being applied is a quantum wire in GaAs containing a shallow δ-doped layer (dotted in Fig. 11). This is incorporated into an FET test structure (O'Neill *et al.* 1993). The quantum wire is a long mesa, 1 μm wide with reactive-ion-etched trenches on either side. Gate contacts are applied outside the trenches. The effect of lateral fields on the quantum wire was investigated by EBIC and it was found that the form of the EBIC linescans across the wire changed with bias, as shown in Figure 12. MC-SET simulations were used to calcu-

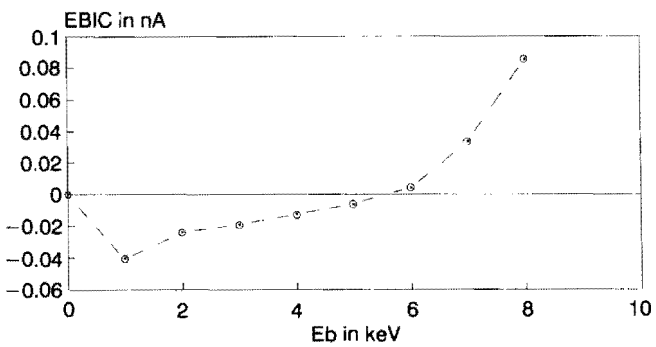

FIG. 10 Variation of EBIC current between contacts to the top and bottom of material with the HEMT structure of Figure 8, as a function of beam energy.

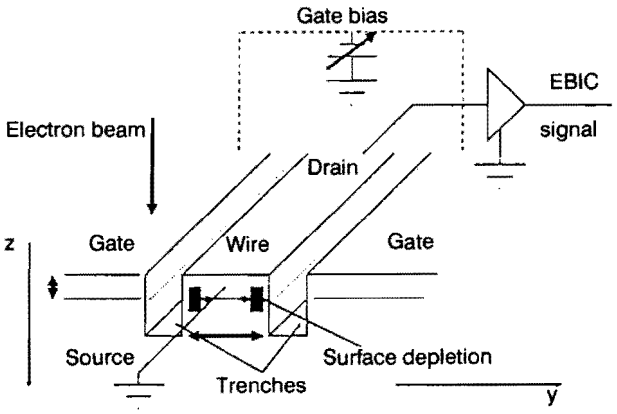

FIG. 11 Structure of a quantum wire FET (O'Neill *et al.* 1993).

late the effect of the escape of beam electrons through the sides of the quantum wire and into the bottom of the trenches and of the backscattered electrons of this type exciting the wire. Noted was that the form of the zero-bias linescan could be accounted for in this way (O'Neill *et al.* 1993). Modeling of the effect of possible depletion regions under the side walls of the quantum wire, induced by the bias field, is now hand.

Discussion

These examples of applications of Monte Carlo simulations to CL and EBIC observations show that the method can quantify a variety of experimental phenomena. At the present time, it is the only such method available except in some simple cases for which reasonable analytic models and the necessary data are available.

The Monte Carlo simulation method is not a substitute or a rival for theory but a simple, practical laboratory tool. It often can be applied to give a first approximation simulation of complex situations for which no full theory or explicit mathematic solution is available and to which it would often be unprofitable to apply theory, for example, particular structures or semiconductor alloys of limited interest. It is not the precision of microcomputer Monte Carlo simulations that is important but their speed and wide applicability that recommend them. In principle, of course, Monte Carlo simulations can be made as accurate as required, provided sufficient computer power is available, as in the work of Oelgart and Werner (1984), Hilbrandt *et al.* (1988), and Phang *et al.* (1992).

References

Bishop HE: Electron-solid interactions and energy dissipation. In *Quantitative Scanning Electron Microscopy* (Eds. Holt DB, Muir MD, Grant PR, Boswarva IM). Academic Press, London (1974) 41–64

Czyzewski Z, Joy DC: Monte-Carlo simulation of CL and EBIC contrasts for isolated dislocations. *Scanning* 12, 5–12 (1990)

Franzosi P, Lazzarini L, Salviati G, Scaffardi M, Fieschi R: Electron-beam-induced dislocations in GaAs and InP single crystals. *J Appl Phys* 66, 2947–2951 (1989)

Garlick GFJ: *Luminescent Materials*. Clarendon Press, Oxford (1949) 175–178

Hilbrandt S, Schreiber J, Hergert W, Petrov VI: Determination of the absorption coefficient and the internal luminescence spectrum of GaAs and $GaAs_{1-x}P_x$ (x = 0.375, 0.78) from beam voltage dependent measurements of cathodoluminescence spectra in the scanning electron microscope. *Phys Stat Sol* (a) 110, 283–291 (1988)

Holt DB, Napchan E, Wojcik A, Ammou M, Gibart P: EBIC in HEMT structures on S.I. substrates. In *Microscopy of Semiconducting Materials 1993*. Inst Phys Conf Ser, Bristol (1993) (in press)

Holt DB, Napchan E, Lazzarini L, Salviati G, Urchulutegui M: Beam-induced dislocations and their CL contrast. In *Microscopy of Semiconducting Materials 1993*. Inst Phys Conf Ser, Bristol (1993) (in press)

Holt DB, Salviati G: Twinning and impurity segregation in Cr- and Fe-doped LEC InP. *J Cryst Growth* 100, 497–507 (1990)

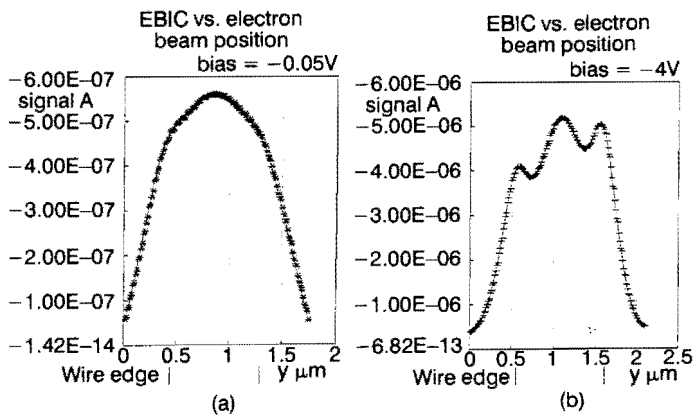

FIG. 12 EBIC line scan profiles across a quantum wire (Fig. 11) with potentials applied to the side gates of (a) −0.05 V and (b) −4 V (O'Neill *et al.* 1993).

Jakubowicz A: Theory of cathodoluminescence contrast from localized defects in semiconductors. *J Appl Phys* 59, 2205–2209 (1986)

Jakubowicz A, Bode M, Habermeier HU: Simultaneous EBIC/CL investigations of dislocations in GaAs. In *Microscopy of Semiconducting Materials 1987*. Inst Phys Conf Ser 87, Bristol (1987) 763–768

Lohnert K, Kubalek E: Characterization of semiconducting materials and devices by EBIC and CL techniques. In *Microscopy of Semiconducting Materials 1983*. Inst Phys Conf Ser 67, Bristol (1983) 303–314

Lohnert K, Kubalek E: The cathodoluminescence contrast formation of localized non-radiative defects in semiconductors. *Phys Stat Sol* (a) 83, 307–314 (1984)

Myklebust RL, Newbury DE, Yakowitz H: A Monte Carlo procedure employing single and multiple scattering. In *Use of Monte Carlo Calculations in EPMA and SEM* (Eds. Heinrich KFJ, Newbury DE, Yakowitz H). NBS Special Publication 460 (1976) 105–128

Napchan E, Holt DB: Application of Monte Carlo simulations in the SEM study of heterojunctions. In *Microscopy of Semiconducting Materials 1987*. Inst Phys Conf Ser 90, Bristol (1987) 733–738

Napchan E: Electron and photon—matter interaction: Energy dissipation and injection level. *Rev de Phys Colloque* C6, C6-15–C6-29 (1989)

Newbury DE.: Modeling electron beam interactions in semiconductors. In *SEM Microcharacterization of Semiconductors* (Eds. Holt DB, Joy DC) Academic Press, London (1989) 29–68

Norman CE, Holt DB: Interpretation of EBIC defect contrast from line defects in silicon. In *Microscopy of Semiconducting Materials 1989*. Inst Phys Conf Ser 100, Bristol (1989) 731–736

Oelgart G, Werner U: Kilovolt electron energy loss distribution in GaAsP. *Phys Stat Sol* (a) 85, 203–213 (1984)

O'Neill DJC, Feng Y, Thornton TJ, Harris JJ: EBIC from δ-doped quantum wires. In *Microscopy of Semiconducting Materials 1993*. Inst Phys Conf Ser, Bristol (1993) (in press)

Pasemann L, Hergert W: A theoretical study of the determination of the depth of a dislocation by combined use of EBIC and CL technique. *Ultramicroscopy* 19, 15–22 (1986)

Phang JCH, Pey KL, Chan DSH: A simulation model for cathodoluminescence in the scanning electron microscope. *IEEE Trans Electr Devices* 39, 782–791 (1992)

Yacobi BG, Holt DB: *Cathodoluminescence Microscopy of Inorganic Solids*. Plenum Press, New York (1990)